HHS Public Access

Author manuscript

J Biomed Mater Res A. Author manuscript; available in PMC 2018 February 08.

Published in final edited form as:

J Biomed Mater Res A. 2016 December ; 104(12): 3058–3072. doi:10.1002/jbm.a.35850.

Elastic, silk-cardiac extracellular matrix hydrogels exhibit time-dependent stiffening that modulates cardiac fibroblast response

Whitney L. Stoppel[1], **Albert E. Gao**[1], **Allison M. Greaney**[1], **Benjamin P. Partlow**[1], **Ross C. Bretherton**[1], **David L. Kaplan**[1], and **Lauren D. Black III**[1,2,*]

[1]Department of Biomedical Engineering, Tufts University, Medford, MA 02155

[2]Cellular, Molecular and Developmental Biology Program, Sackler School of Graduate Biomedical Sciences, Tufts University School of Medicine, Boston, MA 02111

Abstract

Heart failure is the leading cause of death in the United States and rapidly becoming the leading cause of death worldwide. While pharmacological treatments can reduce progression to heart failure following myocardial infarction, there still exists a need for new therapies that promote better healing post injury for a more functional cardiac repair and methods to understand how the changes to tissue mechanical properties influence cell phenotype and function following injury. To address this need, we have optimized a silk-based hydrogel platform containing cardiac tissue-derived extracellular matrix (cECM). These silk-cECM hydrogels have tunable mechanical properties, as well as rate-controllable hydrogel stiffening over time. *In vitro*, silk-cECM scaffolds led to enhanced cardiac fibroblast (CF) cell growth and viability with culture time. cECM incorporation improved expression of integrin an focal adhesion proteins, suggesting that CFs were able to interact with the cECM in the hydrogel. Subcutaneous injection of silk hydrogels in rats demonstrated that addition of the cECM led to endogenous cell infiltration and promoted endothelial cell ingrowth after 4 weeks in vivo. This naturally derived silk fibroin platform is applicable to the development of more physiologically relevant constructs that replicate healthy and diseased tissue *in vitro* and has the potential to be used as an injectable therapeutic for cardiac repair.

Keywords

Silk fibroin; hydrogels; decellularized extracellular matrix; cardiac fibroblasts; integrin expression

1. INTRODUCTION

Cardiovascular disease is the leading cause of death in the U.S.[1] and is rapidly becoming the leading cause of death worldwide.[2] While the initial remodeling that occurs in cardiac tissue following myocardial infarction (MI) is beneficial in preventing ventricular rupture and stabilizing the injured region,[3] continued remodeling leads to increased ventricular compliance, pathological hypertrophy of the surviving cardiac muscle, and eventual heart

*Corresponding Author: Lauren D. Black III, Ph.D., Department of Biomedical Engineering, Tufts University, 4 Colby Street, Medford, MA 02155, lauren.black@tufts.edu.

failure (HF).[4] HF alone is the cause of over 600,000 deaths per year in the U.S.[1] and leads to a significant financial burden on the U.S. healthcare system.[5] Pharmacological treatments can often slow the progression to HF by reducing the workload on the injured heart,[6,7] but ultimately this only prolongs the time to the eventual functional decline. Thus, there exists a need for new treatments that can assist in preventing the progression to HF following MI, as well as *in vitro* platforms capable of mimicking the disease microenvironment to aid in the development of new drugs or therapies.

Tissue engineering and biomaterials approaches are critical for the development of *in vitro* methods to study the progression of heart failure. There have been a number of approaches for generating tissue-engineered myocardium that could be implanted onto the injured heart over the course of the last 2-3 decades,[8,9] and many more materials have been developed and utilized for modeling cardiac tissue *in vitro*.[8] These tissue engineered grafts or constructs utilize a variety of natural biomaterials including fibrin, collagen, and decellularized heart tissue,[10-12] and synthetic materials, such as poly(glycerol sebacate).[13,14] Synthetic materials that form elastic hydrogels generally have improved tunability in terms of mechanical properties and architecture and controllable degradation rates, but traditionally have issues related to biocompatibility of the degradation products, limited cellular remodeling, and long timelines to clinical approval.[15] Naturally derived biopolymers (including collagen, fibrin, and decellularized extracellular matrix products) are advantageous due to their ability to mimic the binding and adhesion sites of tissue and ease with which cells can remodel the construct, but their *in vivo* application can be limited due to the inability to mimic native mechanical properties and structure.[16]

Silk fibroin is a naturally derived biopolymer with controllable crosslinking density and degradation rates. However, silk fibroin requires either chemical modifications or utilization in a composite with a naturally derived biopolymer to support mammalian cell attachment and remodeling. Recently, we developed a tunable, highly elastic, silk hydrogel, which can be formed via di-tyrosine crosslinks caused by an enzymatic crosslinking approach using horseradish peroxidase (HRP) and H_2O_2[17] and the injectability of this system has been previously investigated for the support and augmentation of cervical tissue.[18] In this system, the reaction rate can be systematically controlled through modulation of the ratio of H_2O_2 to HRP and the crosslinking density can be controlled by the overall concentration of HRP added.[17,18] Given the mechanism of silk fibroin hydrogel formation and the proven advantages of decellularized extracellular matrix products,[19-22] we hypothesize that silk fibroin-decellularized ECM composite hydrogels are an ideal material for the development of *in vitro* models of disease or development.

To investigate this hypothesis, we created a composite system composed of silk fibroin and porcine derived cardiac extracellular matrix (cECM). Our previous work in creating pre-formed silk-cECM sponges demonstrated that this composite approach is feasible and that the incorporation of cECM into silk scaffolds promoted better cell function *in vitro* and enhanced cell infiltration *in vivo*.[31] Here we expand upon our recently developed, tunable, highly elastic, silk hydrogel[17] and demonstrate that by altering the silk parameters (e.g., molecular weight via extraction time or concentration), both the gelation kinetics and modulus of the hydrogels can be altered. In addition, we show that cell culture conditions

lead to time-dependent stiffening of the hydrogels in culture, which is independent of cell encapsulation. Through the addition of cECM, we promote cell attachment and integrin activity within the hydrogels, improving cardiac fibroblast viability and altering protein expression as compared to silk hydrogels without any matrix proteins. Silk-cECM hydrogels also show significant cell infiltration and remodeling after 4 weeks post subcutaneous injection.

2. METHODS

All chemicals were purchased from Sigma-Aldrich (St. Louis, MO) unless otherwise noted.

2.1. Silk Solution Preparation

Silk fibroin solution was prepared as reported previously.[23] Briefly, pure silk fibroin was extracted from Bombyx mori cocoons by degumming 5 grams of fibers in 2 L of boiling sodium carbonate solution (0.02 M) for 30 min. The cocoons were first cleaned to remove any remnants of the silk worm using tweezers. Degummed fibers were rinsed three times with distilled water and air-dried in a chemical hood. The dried fibers were then solubilized in aqueous lithium bromide (9.3 M) at 60 °C for 4 hours. The solution was dialyzed using Slide-A-Lyzer Dialysis Cassettes (3500 MWCO, ThermoScientific, Rockford, IL) against reverse osmosis deionized water until the conductivity of the dialysis water was <10 mS cm^{-1} (indicative of complete lithium bromide removal). Centrifugation was used to remove insoluble particulates (9700 RPM, 20 min, 4 °C). To prepare the solution for *in vitro* culture, it was poured into a glass bottle and autoclaved for 20 minutes on a liquid cycle (18 psi, 121 °C, 20 min sterilization cycle). Following autoclaving, the solution was centrifuged two more times to remove any insolubilized silk or particulates. The final concentration of the silk solution was determined by drying a known volume of the solution and massing the remaining solids. This protocol resulted in a 4.5-6% wt v^{-1} silk solution. Silk solutions were stored at 4 °C for a maximum of 2 weeks.

2.2. Cardiac Extracellular Matrix Isolation

Adult porcine hearts were obtained from the local abattoir. Only the left ventricular tissue was utilized for matrix collection. Cardiac extracellular matrix (cECM) was decellularized and prepared as previously described.[24] Briefly, cECM was decellularized using 1% sodium dodecyl sulfate (SDS) which removed all of the cellular material, yielding ECM that was white in color. Then, the ECM was rinsed for 2 hours in 0.1% Triton-100 followed by 2-3 days of rinsing in deionized water to remove all of the remaining SDS. This method has previously been demonstrated to remove most of the DNA present in the tissue, yielding only ECM proteins.[25] Then, cECM was lyophilized and milled into a fine powder (< 40 mm^2 particulates). The powder was solubilized by a pepsin-based enzymatic digestion in 0.1 M HCl for 12 hours. The solubilized myocardial matrix was adjusted to a pH of 10 with 1 M NaOH to inactivate the pepsin and then adjusted to pH 7.4 with 0.1 M HCl and lyophilized for storage. Solubilized cECM powder was reconstituted at 10-30 mg cECM/mL DI water prior to use in hydrogel preparation. For incorporation into silk hydrogels, cECM was added to the silk solution and slowly stirred for 10 min prior to activation of hydrogel crosslinking.

2.3. Silk hydrogel formation

Hydrogels were prepared via modification to previously reported methods.[17] Briefly, polydimethylsiloxane (PDMS) was utilized to secure Tygon® R-3603 tubing with an inner diameter of 7.9 mm (5/16 inches), generating cylindrical molds, formed from materials that do not interact with silk hydrogel formation, enabling easy removal of the formed hydrogels from their molds. Hydrogels were formed according to the formulations in Table 1 and pipetted into the tube molds (400 μl/sample). The first four items listed in Table 1 were mixed together gently by falcon tube inversion or via slow stirring and the remaining volume was accounted for via the addition of deionized water. If cells were added to the formulation, the amount of water needed was reduced to account for the volume of cell suspension added.

Dulbecco's Modified Eagles Medium (DMEM powder, Life Technologies) was prepared at 10× concentration, with the addition of sodium bicarbonate (3.7 g/L at 1×), antibiotic/antimycotic solution (Life Technologies), L-glutamine (Life Technologies), sodium pyruvate (Life Technologies), 20 mM HEPES buffer, and 10 mM ascorbic acid to maintain the 10× concentrations needed in the stock solution.

2.4. Mechanical property measurements and calculations

Unconfined compression tests were conducted to assess the role of silk concentration, silk molecular weight, and cECM addition on the mechanical properties of silk hydrogels. Elastic recovery was evaluated via a single compression cycle. Hydrogels were loaded in a TA Instruments RSA3 Dynamic Mechanical Analyzer (TA Instruments, New Castle, DE) between stainless steel parallel plates. The stress response to an increase in strain was monitored at 10% strain/minute for strains between 0 and 35%. In addition, frequency dependence of the hydrogels was assessed at 1% strain for frequencies between 0.1 and 10 Hz.

To calculate the elastic modulus the slope of the stress strain curve was calculated via a linear regression of the data points collected between 20% and 30% strain for all samples and six samples were evaluated for each condition. This strain window was chosen for the calculation of the elastic modulus because it was the only range of strains that were consistently within the linear regime for all samples at all time points ($R^2 > 0.90$). However, we recognize that these strains are much higher than those in a healthy human heart. For that reason, we also calculated the slope of the stress strain curve for each sample at each time point by calculating the tangent to the stress strain curve at 10% and 20% strain (see Supplementary Methods, Results, and Figure 2). To further understand the changes in mechanical properties, an exponential curve was fit to all of the data between strains of 0.05% and 35% as discussed further in supplementary methods, results, and Figures 3 and 4.[26]

2.5. Measurement of gelation kinetics

The kinetics of gel formation was assessed using rheology. Measurements were carried out on a TA Instruments ARES-LS2 rheometer (TA Instruments, New Castle, DE) utilizing a 25mm stainless steel cone (angle: 0.0994 rad) and a temperature controlled Peltier lower plate at 37°C. Hydrogels were mixed according to Table 1 and 420 μL of solution was

loaded onto the rheometer. The geometry was lowered to the appropriate gap and mineral oil was applied around the edge of the cone to minimize water evaporation. A dynamic time sweep was conducted using a frequency of 1 Hz (6.283 rad/sec) with an applied strain of 1%, for 6000 seconds or until the sample had reached a plateau modulus, whichever occurred first.

2.6. Fourier transform infrared spectroscopy (FTIR) analysis

Changes in the secondary structure of the hydrogels were analyzed via a JASCO FTIR 6200 spectrometer (JASCO, Tokyo, Japan) fitted with a MIRacle™ attenuated total reflection (ATR) germanium crystal. Day 0 samples (30 mE) were allowed to gel for 4 hours prior to testing. Day 7 samples were allowed to gel and subsequently soaked in PBS for 7 days with exchange of the buffer on days 3 and 6. In order to eliminate the interference of water in the amide I region, immediately prior to testing samples were soaked in deuterated water for 2 hours with one exchange. Each sample was the average of 32 co-added scans with a resolution of 4 cm^{-1}. Background spectra were collected under the same conditions and subtracted from the sample absorbance.[27]

2.7. Cardiac fibroblast isolation

Cardiac fibroblasts were isolated from healthy, male Sprague Dawley rats (7-8 weeks, ~250 g) following animal protocols approved by Tufts Institutional Animal Care and Use Committee. Briefly, hearts were removed from sacrificed animals (CO_2 asphyxiation) and ventricular tissue was minced, rinsed with PBS, and digested using a 300 units/mL type II collagenase solution (Worthington Biochemical Corporation, Lakewood, NJ) for 30 minutes in a cell culture incubator. Cells were separated from tissue via a 70 um cell strainer and collagenase solution was removed via centrifugation. Cells were re-suspended in supplemented DMEM + Glutamax (Life Technologies) (1× Anti-Anti (Life Technologies), 20% FBS (Gibco), 10 mM acorbic acid) and allowed to attach to the plates for 6 hours before rinsing and removing any non-attached cells. Attached cells were given fresh media and left undisturbed for 48 hours to promote cell growth and proliferation. By removing unattached cells after 6 hours, the population was restricted to highly adherent cells due to the issues cardiomyocytes have in attaching to uncoated tissue culture plastic. Cells were passaged every 4-6 days and fed every 2-3 days. Cells were used at passages 3-4 for these experiments. Vimentin, N-cadherin, and vinculin staining was used to confirm the CF population (Supplementary Figure 1), which was consistent with reports in the literature.[28]

2.8. Cardiac fibroblast activation

CFs were activated during the first 48 hours of culture within the silk hydrogels via delivery of soluble transforming growth factor beta (TGF-β1, 2.5 ng/mL)[29] in the culture medium (#100-21, PeproTech). Activation of the CFs was performed to increase their proliferation and alpha smooth muscle actin (α-SMA) production within the system, mimicking a disease or injury environment such as that found following myocardial infarction, during atherosclerosis, or in other forms of cardiomyopathy.[30,31] Following 48 hours, hydrogels were rinsed with PBS and then cultured in serum-free DMEM + Glutamax (Life Technologies) supplemented with 1× Anti-Anti (Life Technologies), 10 mM ascorbic acid,

1× ITS (insulin transferrin selenium), and 1:1000 chemically defined lipid concentrate (Gibco).

2.9. Isolation of protein and DNA

Fisher BioReagents™ SurePrep™ RNA/DNA/Protein Purification Kit (Fisher Scientific, Waltham, MA) was utilized to collect RNA, DNA, and protein from each of the hydrogels. Prior to isolation steps, hydrogels were cut into 4 pieces and flash frozen in liquid nitrogen. Hydrogels were digested with the provided lysis buffer using a vibrating tissue dissociator as directed for tissue samples. In some cases, extra time was added to the centrifugation steps in the protocol to ensure that the entire sample was processed through the provided spin columns.

Total protein content in each sample was analyzed via a Pierce BCA Protein Assay (ThermoFisher Scientific, Waltham, MA) to determine the loading necessary for western blot analysis. RNA purity and concentration was determined using a NanoDrop (ThermoFisher Scientific, Waltham, MA). Genomic DNA content was also measured on the NanoDrop. In all cases, relative amounts are reported, using the silk only hydrogel as the control.

2.9.1. Analysis of protein expression via western blot analysis—In order to assess the potential cell signaling pathways involved in cECM incorporation into silk scaffolds, pathways previously implicated in proliferation and cell survival were evaluated by Western blot techniques previously described by our lab.[32] Equal amounts of protein (12 μg per lane) were loaded into pre-cast 4–12% polyacrylamide gels (456-1086) and run before being transferred to a nitrocellulose membrane. Primary antibodies were used to evaluate the expression of the various proteins over time (day 2 and day 6) and for each condition. β-actin was utilized to normalize to total cell content. Antibodies were used at a 1/1000 dilution for primary antibodies and a 1/5000 dilution for secondary antibodies. Species-specific secondary antibodies conjugated to HRP (cat #s 656120 and 656520, Invitrogen, Carlsbad, CA) were used for enhanced chemiluminescence. Images were acquired on the G:Box Chemi XR5 (Syngene, Cambridge, United Kingdom). Expression intensities were analyzed using ImageJ (NIH, Bethesda, MD). Expression intensities for each protein were normalized to the mean expression intensity per blot for that respective protein to allow for comparison between blots.

2.10. *In vivo* subcutaneous analyses

All procedures were conducted under animal protocols approved by Tufts Institutional Animal Care and Use Committee. All animals used in this study were 6–7 week old Sprague Dawley rats (Charles River Laboratories, Wilmington, MA). Silk hydrogel systems (Table 1, where cell culture media was replaced by PBS) were subcutaneously injected into lateral pockets of each rat under general anesthesia of oxygen and isoflurane 15 minutes following the addition of H_2O_2 to the solution. At week 4 post-implantation, animals were euthanized and the samples along with the overlaying tissue were collected for histological examination.

2.11. Histochemical analysis of hydrogels injected subcutaneously

In vivo sections were stained with hematoxylin (Sigma-Aldrich, St. Louis, MO) to visualize cell nuclei and Masson's Trichrome (Sigma-Aldrich, St. Louis, MO) to visualize collagen deposition (blue), muscle fibers and blood vessels (red). Following staining and dehydration, samples were embedded in DPX Mountant (Sigma Aldrich, St. Louis, MO) and imaged using a Keyence® BZ-X700 series microscope. VEGFR-2 (sab4501645, 1/100), CD3 (ab5690, 1/100), CD68 (ab125212, 1/200), CD31 (ab64543, 1/200), alpha smooth muscle actin (sc-32251, 1/200), and C-C chemokine receptor 7 (CCR7, NB100-712, 1/250) antibodies were also used to evaluate cell infiltration in cECM containing hydrogels. Nuclei were stained with DAPI. Secondary visualization of the primary antibodies was completed with Alexa Fluor® 488 goat anti-mouse (Thermofisher, A11001), Alexa Fluor® 555 donkey anti-rabbit (Thermofisher, A31572), and Alexa Fluor® 488 donkey anti-goat (Thermofisher, A11055).

2.12. Statistical analysis

A three-way ANOVA was used to determine the significance of silk concentration, cECM concentration, and culture time and post-hoc Tukey testing was used to determine the additive effects of these parameters. Significance was defined as $p < 0.05$.

3. RESULTS

3.1. Quantification of the mechanical properties of cell-free silk fibroin – ECM composite hydrogels indicates a time-dependent stiffening of the system

Measurement of gelation kinetics demonstrated that the HRP- H_2O_2 reaction induces silk hydrogel formation within the first 800 seconds or 13 minutes following addition of H_2O_2 (Figure 1A,B). The gelation process was relatively independent of the extraction time, but somewhat dependent on the silk concentration in solution. The addition of cECM to the mixture had a limited effect on gelation kinetics for any of the silk concentrations or extraction times. Following cell-free hydrogel formation in the presence of both cell culture media and cECM, it was confirmed that the hydrogels were viscoelastic in nature as measured by dynamic mechanical testing, with the dynamic modulus remaining linear over frequencies required for cardiovascular applications (Figure 1C,F). However, over time in culture, the gels demonstrated an increased stiffness and changes to the hysteresis present in their stress-strain relationships. Figure 1D,F shows the progression of the change in mechanical properties, demonstrating that this process occurred slowly over the course of 6 days. After this stiffening had occurred, unconfined compression to 35% strain led to permanent deformation of the hydrogels, regardless of silk extraction time or molecular weight, silk fibroin concentration or cECM incorporation.

Further quantification of the changes in mechanical properties of these hydrogels over time was measured by calculating the elastic modulus of the gels from 20-30% strain (Figure 2), for all variations of silk concentration (2% and 4%), extraction time (10 mE and 30 mE), and ECM incorporation (0, 1.2 and 2.4 mg/ml). cECM incorporation minimally impacted the modulus of the silk-ECM gels, while silk concentration and molecular weight play greater roles in the mechanical properties and the degree and timing of material stiffening (Figure

2). In particular, with a decrease in molecular weight of the silk in solution (equivalent to an increase in extraction time), the silk hydrogels stiffen at a faster rate, stiffening after 4 days in culture as opposed to 6 days for the 10 mE gels. In addition, higher percentages of silk yielded higher moduli (2% vs. 4%).

While the elastic modulus was calculated in the linear range of the stress-strain curve at 20-30% strain, we recognize that this strain value is higher than what is typically found in the heart. To assess potentially biologically relevant mechanical properties, the slope of the stress-strain curve was calculated for all variations of silk concentration (2% and 4%), extraction time (10 mE and 30 mE), and ECM incorporation (0, 1.2 and 2.4 mg/ml) at both 10% and 20% strain. These data are shown in Supplementary Figure 2. To determine if the shapes of the stress-strain curves change over time, an exponential model was fit to the data as described in the Supplementary Materials. Resulting parameter analysis suggests that the shape of the loading curve changes over time, indicating a shift in the viscoelasticity of the material (Supplementary Figures 3 and 4).

3.2. FTIR analysis confirms conformational changes accompany stiffening

To further assess the cause of the stiffening of the acellular gels with time in culture and to specifically test our hypothesis that the increased salt content in the culture medium was leading to changes in silk fibroin secondary structure over time, we subjected the gels to FTIR analysis[27] (Figure 3). There are distinct differences in the spectra of samples tested with and without submersion in PBS, which was used to represent time in cell culture media. After soaking, the peak centered on 1633 cm^{-1} was depressed and there was a narrowing of the peak centered at 1619 cm^{-1}. Additionally, the shoulder located at 1685 cm^{-1} was redshifted to 1695 cm^{-1}.

Due to the changes in silk secondary structure and the changes in inter- and intra-chain behavior within these systems over time, it is necessary to document how the failure of the material changes over time as function of extraction time, concentration, and cECM incorporation. To this end, dynamic loading-unloading cycles were performed at 10% strain/minute and resulting loading and unloading curves are shown in Supplementary Figure 5.

3.3. Cardiac fibroblasts can be encapsulated and grown inside silk-ECM hydrogels

For all cell-based experiments, cells were added to the solution 8 minutes following H_2O_2 addition and then the solution was immediately aliquoted into custom hydrogel molds. This process limited the interaction of the H_2O_2 with the cells, resulting in improved cell viability within these systems (Figure 4B) compared to silk alone (Figure 4A). The addition of cECM to the silk hydrogels allowed for better cell spreading by the CFs in the gels as evident by greater spread area in histological stains of filamentous actin using phalloidin (Figure 4E, 4F). DNA content significantly increased between day 2 and day 6 for all 10 mE silk samples and addition of cECM significantly increased the DNA content after 6 days within 10 mE silk samples (Figure 4C). Similarly, DNA content significantly increased after 6 days in culture for all 30 mE samples (Figure 4D). However, the increase in stiffness within the 4% 30 mE silk samples limited the increase in DNA content over time (Figure 4D). Importantly, the addition of cECM to the silk hydrogels allowed for better cell spreading by

the CFs in the gels as evident by greater spread area in histological stains of filamentous actin using phalloidin (Figure 4F compared to silk only in Figure 4E).

3.4. Cardiac fibroblasts are able to interact with the cECM in the hydrogels and protein expression is modulated by the changes in stiffness of the silk-ECM composite gel

To promote a myoblast-like phenotype of the CFs that is typically present in the infarct region, hydrogels were cultured in cell culture media supplemented with TGF-β1 for 48 hours and then switched to normal growth medium. Protein expression was then analyzed on day 2 and 6 for the various hydrogel formulations (Figures 5 and 6). Alpha smooth muscle actin expression remained the same in silk hydrogels without cECM formed with 10 mE silk (Figure 5A), while expression was comparatively significantly decreased after 6 days in 30 mE silk (Figure 5B). When cECM was introduced, overall α-smooth muscle actin expression increased between day 2 and day 6 in culture for the 10 mE silk. Similar trends are seen with the addition of cECM to the silk hydrogels formed with 30 mE silk (Figure 5B), but the fold change in protein expression is 2 fold lower for these samples suggesting that the 10 mE silk-cECM hydrogels enhance α-smooth muscle actin compared to the 30 mE silk-cECM samples. Analysis of vinculin expression by CFs in this system demonstrated that samples with a higher silk concentration had a greater expression of this focal adhesion protein both at day 2 and day 6 (Figure 5C, D) for 10mE silk hydrogels. In general, vinculin expression was also reduced in the 30mE samples as compared to the 10mE samples. For all groups there appeared to me a minimal effect of ECM concentration on vinculin expression.

β1 integrin and integrin linked kinase (ILK) trend toward an increase in expression in all of the gel formulations with time in culture (Figure 6). Specifically, the 4% silk formulations at day 6 had the highest values for ILK expression for each of the cECM concentrations and in the 30 mE samples there was a significant increase in ILK expression with increasing concentrations of cECM in all silk formulations (Figure 6B). In contrast there appeared to be little to no effect of cECM concentration on ILK expression in the 10 mE samples (Figure 6A). In the 10 mE silk samples, β1 integrin expression increases significantly with time and concentration of cECM, suggesting that cell growth, stiffness, and cECM incorporation positively influenced β1 integrin expression. On the contrary, an increase in stiffness (30 mE) limited the fold change in β1 integrin expression with the addition of cECM as shown by the comparison between Figure 6C and Figure 6D. However, cECM addition still positively affected β1 integrin expression.

3.5. Silk-cECM hydrogels as injectable materials

In vivo analysis of silk-cECM hydrogels as injectable materials was performed by mixing the components in Table 1, drawing them up into a syringe, and injecting them into the subcutaneous region on the backs of male Sprague Dawley rats. Histological analysis of samples recovered after 4 weeks shows that cECM incorporation improves cell infiltration and vascularization within the hydrogels compared to silk alone (Figure 7). While all formulations were tested, representative images of 4% silk and 4% silk + 2.4 mg/mL cECM are presented, where the left column shows a full sample (Figures 7A, 7D, 7G, 7J), the middle column shows an image from the middle of the hydrogel (Figures 7B, 7E, 7H, 7K), and the right column shows the tissue-hydrogel interface (Figures 7C, 7F, 7I, 7L). In each

case, sections are stained with hematoxylin and eosin (Figure 7ABC and 7GHI) to qualitatively show an increase in cell infiltration and an increase in cellular remodeling compared to silk hydrogels injected without ECM, which is consistent with previously reported results.[17,18] Representative silk (Figure 7DEF) and silk-cECM (Figure 7JKL) hydrogels are stained with Masson's trichrome to evaluate ECM production and cell infiltration. Figure 7J, 7K, and 7L show the existence of ECM proteins within the silk-cECM hydrogels and suggest that cells are able to remodel the hydrogel when it contains ECM. The presence of VEGFR-2, αSMA, and CD31 staining in cECM containing hydrogels injected subcutaneously (Figure 8), demonstrated that some portion of the infiltrating cells were endothelial, fibroblasts, or smooth muscle phenotypes. Of note, there appear to be lumen like structures in CD31 positive cells, further indicating potential vascularization of the injected hydrogel with cECM (yellow arrows in CD31 image and inset). CD31, CCR7, CD68, and CD3 staining shows immune system activation and results suggest that immune cells are also part of the infiltrating population within these silk-cECM hydrogels (Figure 8).

4. DISCUSSION

The creation of new soft hydrogel materials for cardiac tissue engineering aims to enhance the development of novel *in vitro* models of healthy or diseased cardiac tissue, while also potentially leading to novel materials for the *in vivo* delivery of growth factors, therapeutics, or cells in a non-invasive manner. Here, we present a tunable silk-cECM composite system, formed via adaptation of a previously developed protocol[17] that takes advantage of the tyrosine residues in the silk fibroin protein. Using free radical generation by HRP and H_2O_2, di-tyrosine crosslinks form between tyrosines in the silk fibroin protein. We sought to enhance this previous system via the addition of cECM to promote better cellular integration and signaling through adhesive peptides. We demonstrated that the initial mechanical properties of the formed hydrogels can be varied by changing the initial composition of the material (Table 1, Figure 1). Interestingly, these gels exhibit a time-dependent stiffening, even in the absence of cells (Figure 2). This composite gel system is injectable and cECM addition promotes better cellular integration *in vivo* compared to silk alone (Figure 9). Below we discuss the specific findings in the context of the field.

4.1. System design and formulation optimization

Variations in the silk formulation enable the generation of hydrogels with mechanical properties ranging from <5 kPa at the time of formation to up to 40-100 kPa following stiffening (Figure 2, Supplementary Figure 2). Importantly, these values are in line with previous studies reporting the mechanical properties of the developing heart (10-30 kPa) [33] and the stiffness of infarcted heart tissue (40-100 kPa).[34] In addition, the formulations that have a final stiffness value of 40-50 kPa are in the range of injectable gels that have previously demonstrated a functional benefit following injection post-MI.[35] It is also important to note that the observed differences in the initial mechanical properties with changes in the formulation (e.g., cECM addition, autoclaving silk solution for sterilization) were comparable to those previously reported for the highly elastic silk hydrogel.[17,18] This previous system was designed to bulk tissue with minimal cellular infiltration and subsequent degradation.[18] Here we sought to promote cell infiltration in order to alter the

remodeling response both *in vitro* and upon injection *in vivo*. To improve cell viability, infiltration, and activity within these silk hydrogels, we added cECM to provide sites for cell attachment. cECM has been previously shown to promote ckit+ cardiac progenitor cell attachment,[36] as well as vascularization and improved function following injection into infarct tissue *in vivo*.[21] However, it is difficult to control the stiffness of hydrogels formed from solubilized cECM. To combat this, composite PEG-cECM hydrogels have been developed,[37] but these involve the use of a synthetic backbone which has limited degradability. In addition, we also altered the processing of the silk solutions from the previous study in that they were autoclaved prior to use to make sure that all aspects of the system were biocompatible and free of contamination. Other sterilization methods for 10 mE or 30 mE silk fibroin solutions are limited, because the high viscosity of these solutions prevents sterile filtration.[38,39] These changes in solution formulation are important in the timeline and intensity of the reported changes in mechanical behavior compared to previously reported data on silk fibroin hydrogel systems.[17,18]

4.2. Time-dependent gel stiffening and its relevance to cardiac applications

Mechanical and adhesive cues are important for guiding cell growth, function, maturation, and differentiation of a variety of cell types,[40-44] including cardiomyocytes.[33,45,46] In particular, dynamic material cues are important for guiding cardiac cell maturation or for mimicking the change in bulk tissue properties *in vitro* that occur during development[45] or disease.[34] The development of a hydrogel for use as an injectable platform or an *in vitro* model requires an understanding of how the material properties within a system change over time, specifically when the research goal is to mimic a biological environment where mechanical properties are in flux. For example, it is well known that during cardiac development, tissue mechanics change as maturation occurs.[33,4547] In disease, such as atherosclerosis, vessel tissue stiffens due to localized plaque formation, altering the behavior of the smooth muscle cells and pericytes located near the plaque.[48,49] The time-dependent stiffening in this system happens as a result of changes in the silk fibroin secondary structure within the silk systems (Figure 3, Supplementary Figure 5) that occurs over a 2-3 day period (Figure 2, Supplementary Figures 3 and 4). Mimicking the dynamic mechanical changes to the cellular microenvironment that are present in normal development could lead to new biomaterials that enhance the maturation of stem-cell derived cardiomyocytes following injection into the heart. Ultraviolet irradiation or free radical crosslinking have shown that dynamic changes in material properties alter stem cell differentiation and maturation,[50,51] and these materials are implantable for cardiac applications, such as repair post-MI.[52] This is particularly important in cardiac development,[53] where dynamic stiffening has been shown to enhance the differentiation and maturation of embryonic chick cardiomyocytes.[45] Similarly, while the stiffness of the infarct microenvironment has been previously measured and utilized in model systems, materials that mimic dynamic changes in the stiffness would likely serve as ideal materials for *in vitro* model systems mimicking the disease process. Our work is the first step in this process, demonstrating that dynamic changes in stiffness impact the disease response of cardiac fibroblasts through upregulation of myofibroblasts markers.

The culture method utilized for silk hydrogels greatly impacts the secondary conformation of silk fibroin and the overall mechanical properties of the resulting hydrogels. When

cultured in a system where the silk polymer is not in contact with a surface or with tissue culture plastic, we hypothesize that silk fibroin polymers are able to reorganize, driven by thermodynamic forces such as charged-based interaction due to increases in salt concentration[54] and Brownian motion. We hypothesize that differences in the rate of stiffening as a results of the differences in the molecular weight of the silk are partially related to the reduced energy required for beta sheet formation in the lower molecular weight silk hydrogels. Our FTIR data (Figure 3) support the fact that there were conformational changes in the silk following time in culture in both 2% and 4% gels; however, further experiments such as the measurement of silk secondary structure over time via FTIR or circular dichroism are needed to fully assess the mechanism behind these changes, both in the presence and absence of salt.

However, we have demonstrated that in the presence of cECM, CFs (*in* vitro) and infiltrating cells (*in vivo*) are able to reorganize the hydrogel structure through interaction with the cECM components, thus impacting how the silk fibroin interacts with itself and other cECM proteins (*in vitro:* CFs: Figure 4-6; *in vivo*: Figure 7,8). Future work should be aimed at understanding the specific mechanism of the stiffening response in this composite system and whether this mechanism could be controlled via modulation of cECM composition or the ratio of cECM to silk fibroin. As the ratio of silk to cECM decreases, we anticipate that the modulation of the dynamic stiffening and eventual plastic deformation of the material may be altered by cell infiltration and remodeling *in vivo*, eliminating some concern for the generation of an inelastic material for tissue regeneration. However, since cellular remodeling *in vitro* does not occur to the same extent or mechanism as *in vivo*, it will be imperative that future work evaluates the mechanical properties of injected materials over time, necessitating separate formulation optimization for *in vitro* and *in vivo* utilization.

4.3. Cardiac fibroblast protein expression in silk-cECM systems

Cardiac fibroblasts were utilized to study this composite gel system *in vitro* because they are the most prevalent cell type in the infarct environment *in vivo*. Moreover, in this study we chose to activate the CFs to a myofibroblast phenotype via TGF-β1 treatment to better mimic the cellular phenotype present in the infarct microenvironment. Addition of cECM improved expression of cardiac fibroblast (CF) proteins over time (Figure 5). Expression of α-smooth muscle actin increased with time, as expected due to the increase in DNA content (Figure 4). In the 30 mE hydrogels where the stiffness increased most drastically compared to other samples (Figure 2), expression of αSMA was significantly lower without cECM addition. Similar trends are seen with vinculin expression. Overall, cECM addition improved or maintained vinculin expression despite drastic increases in the modulus of the material. cECM addition also improved the integrin activity of the activated CFs within these systems (Figure 6) as shown by enhanced ILK and integrin β1 protein expression. This response to cECM addition in silk systems is similar to previously reported results in silk sponges,[24] where cECM addition improved protein expression of cardiac cells *in vitro* and improved cell infiltration *in vivo.* Overall, these results are complimentary to data in previously reported systems where complex ECM composition[19,20,47] and dynamic mechanical properties[45,51,55] influence cell behavior and protein expression.

4.4. Silk-cECM materials and host response *in vivo*

In vivo subcutaneous injection was chosen for this analysis due to the limited data on the safety and efficacy of the silk-cECM hydrogels *in vivo* (Figure 7). While injection has been performed in non-living tissue and evaluation of silk only hydrogels had been performed,[17,18] the role of cECM addition had yet to be evaluated. Staining of cECM containing samples demonstrated expression of vascular endothelial growth factor receptor 2 (VEGFR-2) in the center of the hydrogel volume (Figure 8A). The presence of CD31 (PECAM-1, Figure 8C), a small degree of α-smooth muscle actin (Figure 8B), along with VEGFR-2, suggest that cECM addition promotes cell infiltration and vascularization of these injected hydrogels. Furthermore, the presence of apparent lumens in the CD31 stained images (yellow arrows in image and inset) also support this. VEGFR-2 (KDR) staining identifies cells expressing the VEGF-A receptor, which has been implicated in a variety of vessel growth and regeneration mechanisms, including both blood vessel growth and the development or growth of lymphatic vessels.[56-59] In terms of regeneration and cell infiltration for future applications of these hydrogels, both blood and lymphatic vessel systems are necessary for the integration of the implant with surrounding tissue and therefore expression is an indication of infiltration endothelial precursors. In chronic models of skeletal muscle ischemia, only regenerative cells express VEGFR-2,[59] suggesting that the silk-cECM hydrogels are capable of promoting infiltration of regenerating cell types. αSMA is a known marker for activated fibroblasts, which have a spatiotemporal role in the wound healing cascade.[30] Activated fibroblasts are expected at the site of injury; however, they can be detrimental host-material interactions due to their role in the generation of a fibrous capsule surrounding the material.[60] In Figure 8B, very limited numbers of αSMA positive cells are found in the silk-cECM hydrogels, suggesting that the silk-cECM formulation does not elicit a prolonged activated fibroblast response. CD31 (PECAM) expression in Figure 8C show the presence of lumens, suggesting that some of the $CD31^+$ may be contributing to the development of vasculature. In addition to promoting vascularization, CD31 is also present on activated CD4+ T-cells and can contribute to leukocyte detachment and platelet activation.[61] Recent work suggests that CD31 is required for T-cell survival during response to infection;[62] thus, further analysis of the cues within the cECM that may contribute to T-cell activation and the role that activated T-cells play in host response to these silk-cECM biomaterials will be necessary.

Exploration of host response to biomaterials, whether injectable or implantable, are paramount in determining how the material will alter the local environment. Activation of the immune system to direct remodeling, reduce inflammation, and promote healing are now widely seen as major advantages to biomaterials *in vivo*.[63] To evaluate system host response to our injectable silk-cECM hydrogels, we evaluated macrophage infiltration within the silk-cECM hydrogels in combination with vascular markers to see how the host response altered the remodeling of the hydrogel 4-weeks post subcutaneous implantation. CD3 (Figure 8E) is a known marker of T-cell activation, which is important in the foreign body response to materials. CD68 (Figure 8F) is a pan-macrophage marker, staining macrophages regardless of their activated state. M1 macrophages have previously been shown to upregulate chemokine receptor 7 (CCR7, CD197, Figure 8D),[64] a cell surface marker responsible for activation of both B cells and T cells. CCR7 staining was limited and sparser across the

sample, compared to CD68 and CD3 expression within the silk-cECM hydrogels, where clusters of positively stained cells could be found (Figure 8E). Results demonstrate the complex role of the immune system in promoting cell infiltration and remodeling, where macrophage infiltration and activation can have positive effects on future biomaterial vascularization.[64] Future work should evaluate the timeline over which this immune cell infiltration occurs, which will be critical for determining the long-term inflammatory response to silk-cECM hydrogel materials.

5. CONCLUSIONS

In summary, using silk hydrogels as a modulator of mechanics, and cECM peptides as cell adhesive ligands, we are able to generate materials that stiffen over time while maintaining cellular adhesion to the material. These silk hydrogel systems are formed by free-radical crosslinking of tyrosines within silk fibroin and porcine derived left ventricular extracellular matrix (cECM) and the resulting hydrogels have tunable mechanical properties and promote cell attachment within the hydrogel system. Addition of cECM to silk hydrogels improves cardiac fibroblast protein expression, growth, and viability within the all-natural silk *in vitro* system. Further evaluation via subcutaneous injection of silk-cECM hydrogels in Sprague Dawley rats demonstrates the feasibility of using these hydrogels as injectable systems *in vivo*. Addition of cECM further improves cell infiltration and vascularization *in vivo*, suggesting that this silk-cECM hydrogel platform has many potential uses both *in vitro* and *in vivo*.

Supplementary Material

Refer to Web version on PubMed Central for supplementary material.

Acknowledgments

WLS would like to acknowledge funding from the National Institutes of Health Institutional Research and Academic Career Development Awards program at Tufts University (K12GM074869, Training in Education and Critical Research Skills (TEACRS)). In addition, AMG, who is now completing her graduate work in the Biomedical Engineering Department at Yale University, would like to acknowledge the American Heart Association Summer Fellowship program. BPP acknowledges funding from the National Defense Science and Engineering Graduate Fellowship. RCB acknowledges funding from the Tufts University Summer Scholars Research Fellowship Program. We also thank the NIH P41 (EB002520) for support of this work.

References

1. Mozaffarian D, Benjamin EJ, Go AS, Arnett DK, Blaha MJ, Cushman M, de Ferranti S, Despres JP, Fullerton HJ, Howard VJ, et al. Heart disease and stroke statistics–2015 update: a report from the American Heart Association. Circulation. 2015; 131(4):e29–322. [PubMed: 25520374]
2. Shepard D, VanderZanden A, Moran A, Naghavi M, Murray C, Roth G. Ischemic Heart Disease Worldwide, 1990 to 2013: Estimates From the Global Burden of Disease Study 2013. Circulation: Cardiovascular Quality and Outcomes. 2015; 8(4):455–456. [PubMed: 26152681]
3. Voorhees AP, DeLeon-Pennell KY, Ma Y, Halade GV, Yabluchanskiy A, Iyer RP, Flynn E, Cates CA, Lindsey ML, Han HC. Building a better infarct: Modulation of collagen cross-linking to increase infarct stiffness and reduce left ventricular dilation post-myocardial infarction. J Mol Cell Cardiol. 2015; 85:229–39. [PubMed: 26080361]

4. Zile MR, Brutsaert DL. New Concepts in Diastolic Dysfunction and Diastolic Heart Failure: Part I: Diagnosis, Prognosis, and Measurements of Diastolic Function. Circulation. 2002; 105(11):1387–1393. [PubMed: 11901053]
5. Heidenreich PA, Trogdon JG, Khavjou OA, Butler J, Dracup K, Ezekowitz MD, Finkelstein EA, Hong Y, Johnston SC, Khera A, et al. Forecasting the Future of Cardiovascular Disease in the United States: A Policy Statement From the American Heart Association. Circulation. 2011
6. Arnold JMO, Yusuf S, Young J, Mathew J, Johnstone D, Avezum A, Lonn E, Pogue J, Bosch J, on behalf of the HI. Prevention of Heart Failure in Patients in the Heart Outcomes Prevention Evaluation (HOPE) Study. Circulation. 2003; 107(9):1284–1290. [PubMed: 12628949]
7. Zile MR, Brutsaert DL. New Concepts in Diastolic Dysfunction and Diastolic Heart Failure: Part II: Causal Mechanisms and Treatment. Circulation. 2002; 105(12):1503–1508. [PubMed: 11914262]
8. Stoppel WL, Kaplan DL, Black LD 3rd. Electrical and mechanical stimulation of cardiac cells and tissue constructs. Adv Drug Deliv Rev. 2016; 96:135–55. [PubMed: 26232525]
9. Reis LA, Chiu LL, Feric N, Fu L, Radisic M. Biomaterials in myocardial tissue engineering. J Tissue Eng Regen Med. 2014
10. Roura S, Soler-Botija C, Bago JR, Llucia-Valldeperas A, Fernandez MA, Galvez-Monton C, Prat-Vidal C, Perea-Gil I, Blanco J, Bayes-Genis A. Postinfarction Functional Recovery Driven by a Three-Dimensional Engineered Fibrin Patch Composed of Human Umbilical Cord Blood-Derived Mesenchymal Stem Cells. Stem Cells Transl Med. 2015; 4(8):956–66. [PubMed: 26106218]
11. Momtahan N, Sukavaneshvar S, Roeder BL, Cook AD. Strategies and Processes to Decellularize and Recellularize Hearts to Generate Functional Organs and Reduce the Risk of Thrombosis. Tissue Engineering Part B-Reviews. 2015; 21(1):115–132. [PubMed: 25084164]
12. Wang RM, Christman KL. Decellularized myocardial matrix hydrogels: in basic research and preclinical studies. Advanced drug delivery reviews. 2016; 96:77–82. [PubMed: 26056717]
13. Neal RA, Jean A, Park H, Wu PB, Hsiao J, Engelmayr GC Jr, Langer R, Freed LE. Three-Dimensional Elastomeric Scaffolds Designed with Cardiac-Mimetic Structural and Mechanical Features. Tissue Engineering Part A. 2013; 19(5–6):793–807. [PubMed: 23190320]
14. Park H, Larson BL, Kolewe ME, Vunjak-Novakovic G, Freed LE. Biomimetic scaffold combined with electrical stimulation and growth factor promotes tissue engineered cardiac development. Experimental Cell Research. 2014; 321(2):297–306. [PubMed: 24240126]
15. Stoppel WL, Ghezzi CE, McNamara SL, Black LD 3rd, Kaplan DL. Clinical applications of naturally derived biopolymer-based scaffolds for regenerative medicine. Ann Biomed Eng. 2015; 43(3):657–80. [PubMed: 25537688]
16. Tan H, Marra KG. Injectable, Biodegradable Hydrogels for Tissue Engineering Applications. Materials. 2010; 3(3):1746–1767.
17. Partlow BP, Hanna CW, Rnjak-Kovacina J, Moreau JE, Applegate MB, Burke KA, Marelli B, Mitropoulos AN, Omenetto FG, Kaplan DL. Highly Tunable Elastomeric Silk Biomaterials. Advanced Functional Materials. 2014; 24(29):4615–4624. [PubMed: 25395921]
18. Brown JE, Partlow BP, Berman AM, House MD, Kaplan DL. Injectable silk-based biomaterials for cervical tissue augmentation: an in vitro study. American Journal of Obstetrics and Gynecology. 2016; 214(1)
19. Williams C, Budina E, Stoppel WL, Sullivan KE, Emani S, Emani SM, Black LD 3rd. Cardiac extracellular matrix-fibrin hybrid scaffolds with tunable properties for cardiovascular tissue engineering. Acta Biomater. 2015; 14(0):84–95. [PubMed: 25463503]
20. Williams C, Quinn KP, Georgakoudi I, Black LD 3rd. Young developmental age cardiac extracellular matrix promotes the expansion of neonatal cardiomyocytes in vitro. Acta Biomater. 2014; 10(1):194–204. [PubMed: 24012606]
21. Seif-Naraghi SB, Singelyn JM, Salvatore MA, Osborn KG, Wang JJ, Sampat U, Kwan OL, Strachan GM, Wong J, Schup-Magoffin PJ, et al. Safety and efficacy of an injectable extracellular matrix hydrogel for treating myocardial infarction. Sci Transl Med. 2013; 5(173):173ra25.
22. Wassenaar JW, Gaetani R, Garcia JJ, Braden RL, Luo CG, Huang D, DeMaria AN, Omens JH, Christman KL. Evidence for Mechanisms Underlying the Functional Benefits of a Myocardial Matrix Hydrogel for Post-MI Treatment. Journal of the American College of Cardiology. 2016; 67(9):1074–1086. [PubMed: 26940929]

23. Rockwood DN, Preda RC, Yucel T, Wang X, Lovett ML, Kaplan DL. Materials fabrication from Bombyx mori silk fibroin. Nat Protoc. 2011; 6(10):1612–31. [PubMed: 21959241]
24. Stoppel WL, Hu D, Domian IJ, Kaplan DL, Black LD 3rd. Anisotropic silk biomaterials containing cardiac extracellular matrix for cardiac tissue engineering. Biomed Mater. 2015; 10(3):034105. [PubMed: 25826196]
25. Singelyn JM, DeQuach JA, Seif-Naraghi SB, Littlefield RB, Schup-Magoffin PJ, Christman KL. Naturally derived myocardial matrix as an injectable scaffold for cardiac tissue engineering. Biomaterials. 2009; 30(29):5409–5416. [PubMed: 19608268]
26. Black LD, Brewer KK, Morris SM, Schreiber BM, Toselli P, Nugent MA, Suki B, Stone PJ. Effects of elastase on the mechanical and failure properties of engineered elastin-rich matrices. J Appl Physiol (1985). 2005; 98(4):1434–41. [PubMed: 15640390]
27. Hu X, Kaplan D, Cebe P. Determining Beta-Sheet Crystallinity in Fibrous Proteins by Thermal Analysis and Infrared Spectroscopy. Macromolecules. 2006; 39(18):6161–6170.
28. Souders CA, Bowers SL, Baudino TA. Cardiac fibroblast: the renaissance cell. Circulation Research. 2009; 105(12):1164–1176. [PubMed: 19959782]
29. Thannickal VJ, Lee DY, White ES, Cui Z, Larios JM, Chacon R, Horowitz JC, Day RM, Thomas PE. Myofibroblast Differentiation by Transforming Growth Factor-β1 Is Dependent on Cell Adhesion and Integrin Signaling via Focal Adhesion Kinase. Journal of Biological Chemistry. 2003; 278(14):12384–12389. [PubMed: 12531888]
30. Shinde AV, Frangogiannis NG. Fibroblasts in myocardial infarction: a role in inflammation and repair. J Mol Cell Cardiol. 2014; 70:74–82. [PubMed: 24321195]
31. Porter KE, Turner NA. Cardiac fibroblasts: At the heart of myocardial remodeling. Pharmacology & Therapeutics. 2009; 123(2):255–278. [PubMed: 19460403]
32. Morgan KY, Black LD 3rd. Mimicking isovolumic contraction with combined electromechanical stimulation improves the development of engineered cardiac constructs. Tissue Eng Part A. 2014; 20(11–12):1654–67. [PubMed: 24410342]
33. Jacot JG, Martin JC, Hunt DL. Mechanobiology of cardiomyocyte development. Journal of Biomechanics. 2010; 43(1):93–98. [PubMed: 19819458]
34. Sullivan KE, Quinn KP, Tang KM, Georgakoudi I, Black LD 3rd. Extracellular matrix remodeling following myocardial infarction influences the therapeutic potential of mesenchymal stem cells. Stem Cell Res Ther. 2014; 5(1):14. [PubMed: 24460869]
35. Ifkovits JL, Tous E, Minakawa M, Morita M, Robb JD, Koomalsingh KJ, Gorman JH 3rd, Gorman RC, Burdick JA. Injectable hydrogel properties influence infarct expansion and extent of postinfarction left ventricular remodeling in an ovine model. Proc Natl Acad Sci U S A. 2010; 107(25):11507–12. [PubMed: 20534527]
36. French KM, Boopathy AV, DeQuach JA, Chingozha L, Lu H, Christman KL, Davis ME. A naturally derived cardiac extracellular matrix enhances cardiac progenitor cell behavior in vitro. Acta Biomaterialia. 2012; 8(12):4357–4364. [PubMed: 22842035]
37. Grover GN, Rao N, Christman KL. Myocardial matrix-polyethylene glycol hybrid hydrogels for tissue engineering. Nanotechnology. 2014; 25(1):014011. [PubMed: 24334615]
38. Rnjak-Kovacina J, DesRochers TM, Burke KA, Kaplan DL. The effect of sterilization on silk fibroin biomaterial properties. Macromol Biosci. 2015; 15(6):861–74. [PubMed: 25761231]
39. Gil ES, Park SH, Hu X, Cebe P, Kaplan DL. Impact of sterilization on the enzymatic degradation and mechanical properties of silk biomaterials. Macromol Biosci. 2014; 14(2):257–69. [PubMed: 24519787]
40. Engler AJ, Sen S, Sweeney HL, Discher DE. Matrix elasticity directs stem cell lineage specification. Cell. 2006; 126(4):677–689. [PubMed: 16923388]
41. Khatiwala CB, Kim PD, Peyton SR, Putnam AJ. ECM Compliance Regulates Osteogenesis by Influencing MAPK Signaling Downstream of RhoA and ROCK. Journal of Bone and Mineral Research. 2009; 24(5):886–898. [PubMed: 19113908]
42. Trappmann B, Gautrot JE, Connelly JT, Strange DG, Li Y, Oyen ML, Cohen Stuart MA, Boehm H, Li B, Vogel V, et al. Extracellular-matrix tethering regulates stem-cell fate. Nat Mater. 2012; 11(7): 642–9. [PubMed: 22635042]

43. Rosenfeld D, Landau S, Shandalov Y, Raindel N, Freiman A, Shor E, Blinder Y, Vandenburgh HH, Mooney DJ, Levenberg S. Morphogenesis of 3D vascular networks is regulated by tensile forces. Proceedings of the National Academy of Sciences. 2016; 113(12):3215–3220.
44. Huebsch N, Arany PR, Mao AS, Shvartsman D, Ali OA, Bencherif SA, Rivera-Feliciano J, Mooney DJ. Harnessing traction-mediated manipulation of the cell/matrix interface to control stem-cell fate. Nat Mater. 2010; 9(6):518–26. [PubMed: 20418863]
45. Young JL, Engler AJ. Hydrogels with time-dependent material properties enhance cardiomyocyte differentiation in vitro. Biomaterials. 2011; 32(4):1002–9. [PubMed: 21071078]
46. Galie PA, Khalid N, Carnahan KE, Westfall MV, Stegemann JP. Substrate stiffness affects sarcomere and costamere structure and electrophysiological function of isolated adult cardiomyocytes. Cardiovascular Pathology. 2013; 22(3):219–227. [PubMed: 23266222]
47. Gershlak JR, Resnikoff JI, Sullivan KE, Williams C, Wang RM, Black LD 3rd. Mesenchymal stem cells ability to generate traction stress in response to substrate stiffness is modulated by the changing extracellular matrix composition of the heart during development. Biochem Biophys Res Commun. 2013; 439(2):161–6. [PubMed: 23994333]
48. Hahn C, Schwartz MA. The Role of Cellular Adaptation to Mechanical Forces in Atherosclerosis. Arteriosclerosis Thrombosis and Vascular Biology. 2008; 28(12):2101–2107.
49. Zhou J, Hu G, Herring BP. Smooth Muscle-Specific Genes Are Differentially Sensitive to Inhibition by Elk-1. Molecular and Cellular Biology. 2005; 25(22):9874–9885. [PubMed: 16260603]
50. Guvendiren M, Burdick JA. Stiffening hydrogels to probe short- and long-term cellular responses to dynamic mechanics. Nat Commun. 2012; 3:792. [PubMed: 22531177]
51. Mabry KM, Lawrence RL, Anseth KS. Dynamic stiffening of poly(ethylene glycol)-based hydrogels to direct valvular interstitial cell phenotype in a three-dimensional environment. Biomaterials. 2015; 49:47–56. [PubMed: 25725554]
52. Highley CB, Prestwich GD, Burdick JA. Recent advances in hyaluronic acid hydrogels for biomedical applications. Current opinion in biotechnology. 2016; 40:35–40. [PubMed: 26930175]
53. Gershlak JR, Black LD 3rd. Beta 1 integrin binding plays a role in the constant traction force generation in response to varying stiffness for cells grown on mature cardiac extracellular matrix. Exp Cell Res. 2015; 330(2):311–24. [PubMed: 25220424]
54. Yao DY, Dong S, Lu Q, Hu X, Kaplan DL, Zhang BB, Zhu HS. Salt-Leached Silk Scaffolds with Tunable Mechanical Properties. Biomacromolecules. 2012; 13(11):3723–3729. [PubMed: 23016499]
55. Humphrey JD, Dufresne ER, Schwartz MA. Mechanotransduction and extracellular matrix homeostasis. Nature Reviews Molecular Cell Biology. 2014; 15(12):802–812. [PubMed: 25355505]
56. Friedrich EB, Walenta K, Scharlau J, Nickenig G, Werner N. CD34−/CD133+/VEGFR-2+ endothelial progenitor cell subpopulation with potent vasoregenerative capacities. Circulation research. 2006; 98(3):e20–e25. [PubMed: 16439688]
57. Hong Y-K, Lange-Asschenfeldt B, Velasco P, Hirakawa S, Kunstfeld R, Brown LF, Bohlen P, Senger DR, Detmar M. VEGF-A promotes tissue repair-associated lymphatic vessel formation via VEGFR-2 and the α1β1 and α2β1 integrins. The FASEB journal. 2004; 18(10):1111–1113. [PubMed: 15132990]
58. Peichev M, Naiyer AJ, Pereira D, Zhu Z, Lane WJ, Williams M, Oz MC, Hicklin DJ, Witte L, Moore MAS. Expression of VEGFR-2 and AC133 by circulating human CD34+ cells identifies a population of functional endothelial precursors. Blood. 2000; 95(3):952–958. [PubMed: 10648408]
59. Rissanen TT, Vajanto I, Hiltunen MO, Rutanen J, Kettunen MI, Niemi M, Leppänen P, Turunen MP, Markkanen JE, Arve K, et al. Expression of Vascular Endothelial Growth Factor and Vascular Endothelial Growth Factor Receptor-2 (KDR/Flk-1) in Ischemic Skeletal Muscle and Its Regeneration. The American Journal of Pathology. 2002; 160(4):1393–1403. [PubMed: 11943724]
60. Darby IA, Laverdet B, Bonté F, Desmoulière A. Fibroblasts and myofibroblasts in wound healing. Clinical, Cosmetic and Investigational Dermatology. 2014; 7:301–311.

61. Liu L, Shi G-P. CD31: beyond a marker for endothelial cells. Cardiovascular Research. 2012; 94(1):3–5. [PubMed: 22379038]

62. Ross EA, Coughlan RE, Flores-Langarica A, Bobat S, Marshall JL, Hussain K, Charlesworth J, Abhyankar N, Hitchcock J, Gil C, et al. CD31 is required on CD4(+) T cells to promote T cell survival during Salmonella infection. Journal of immunology (Baltimore, Md : 1950). 2011; 187(4):1553–1565.

63. Boehler RM, Graham JG, Shea LD. Tissue engineering tools for modulation of the immune response. BioTechniques. 2011; 51(4):239. -passim. [PubMed: 21988690]

64. Spiller KL, Anfang R, Spiller KJ, Ng J, Nakazawa KR, Daulton JW, Vunjak-Novakovic G. The Role of Macrophage Phenotype in Vascularization of Tissue Engineering Scaffolds. Biomaterials. 2014; 35(15):4477–4488. [PubMed: 24589361]

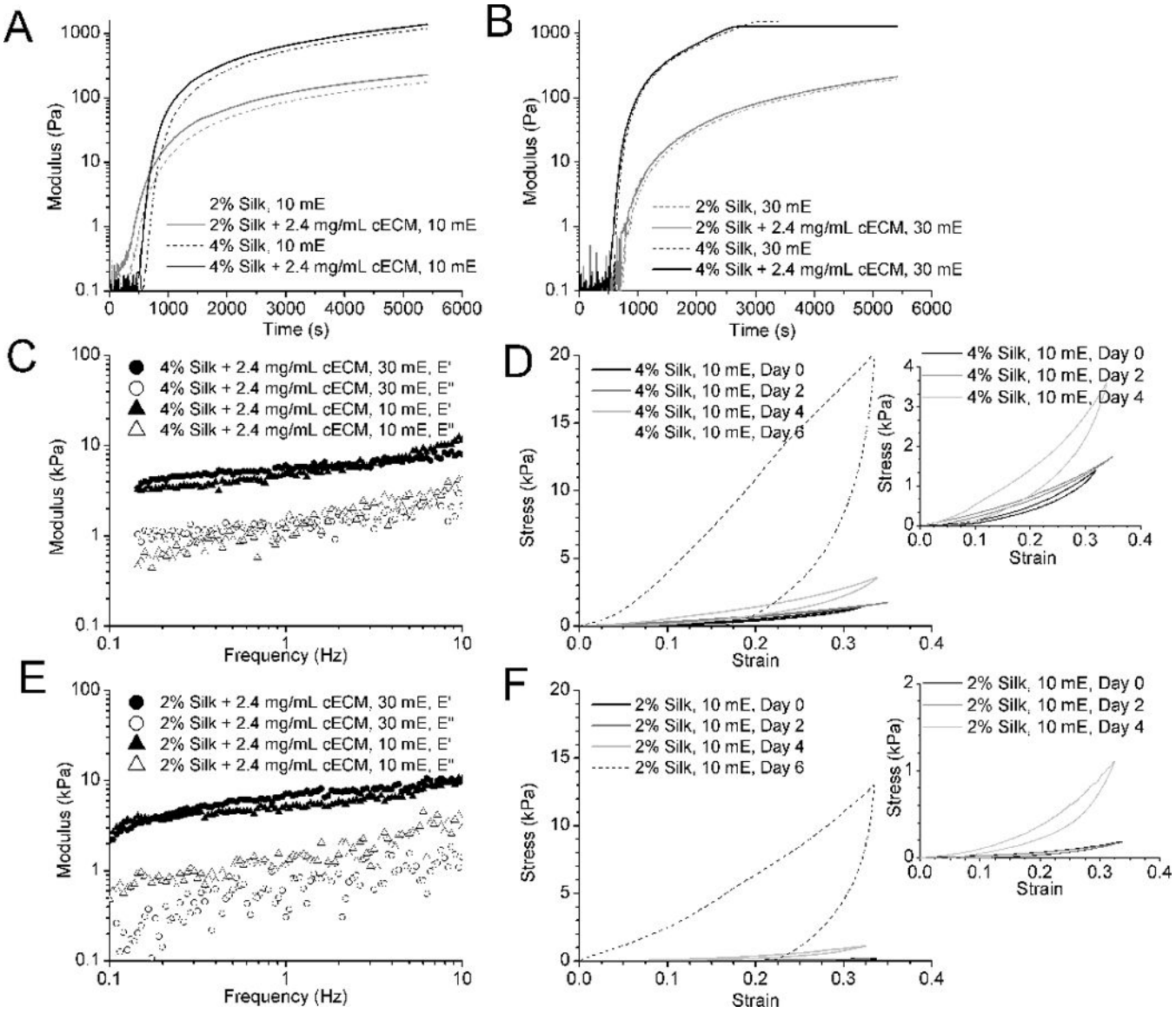

Figure 1. Analysis of hydrogel properties during and post gelation

A) Modulus of 10 minute extracted (mE) silk solution with and without cECM during the gelation shows that addition of cECM (dashed lines) does not significantly delay the gelation of the hydrogels. B) Modulus of 30 mE silk solution with and without cECM during gelation. Both 10 mE and 30 mE silk gelation schemes show a delay in the rise of the modulus, enabling the addition of cells 8 minutes post the initiation of the HRP-H_2O_2 reaction. C) Representative frequency sweep of 10 mE 4% silk with 2.4 mg/mL cECM. D) Stress-strain curves showing the change in relaxation of 10 mE 4% silk hydrogels over time. Representative plots show the loss of full relaxation of the hydrogels as they stiffen over time. The inset plot zooms in on the earlier time points. E) Representative frequency sweep of 10 mE 2% silk with 2.4 mg/mL cECM. F) Stress-strain curves showing the change in relaxation of 10 mE 2% silk hydrogels over time. Representative plots show the loss of full

relaxation of the hydrogels as they stiffen over time. The inset plot zooms in on the earlier time points.

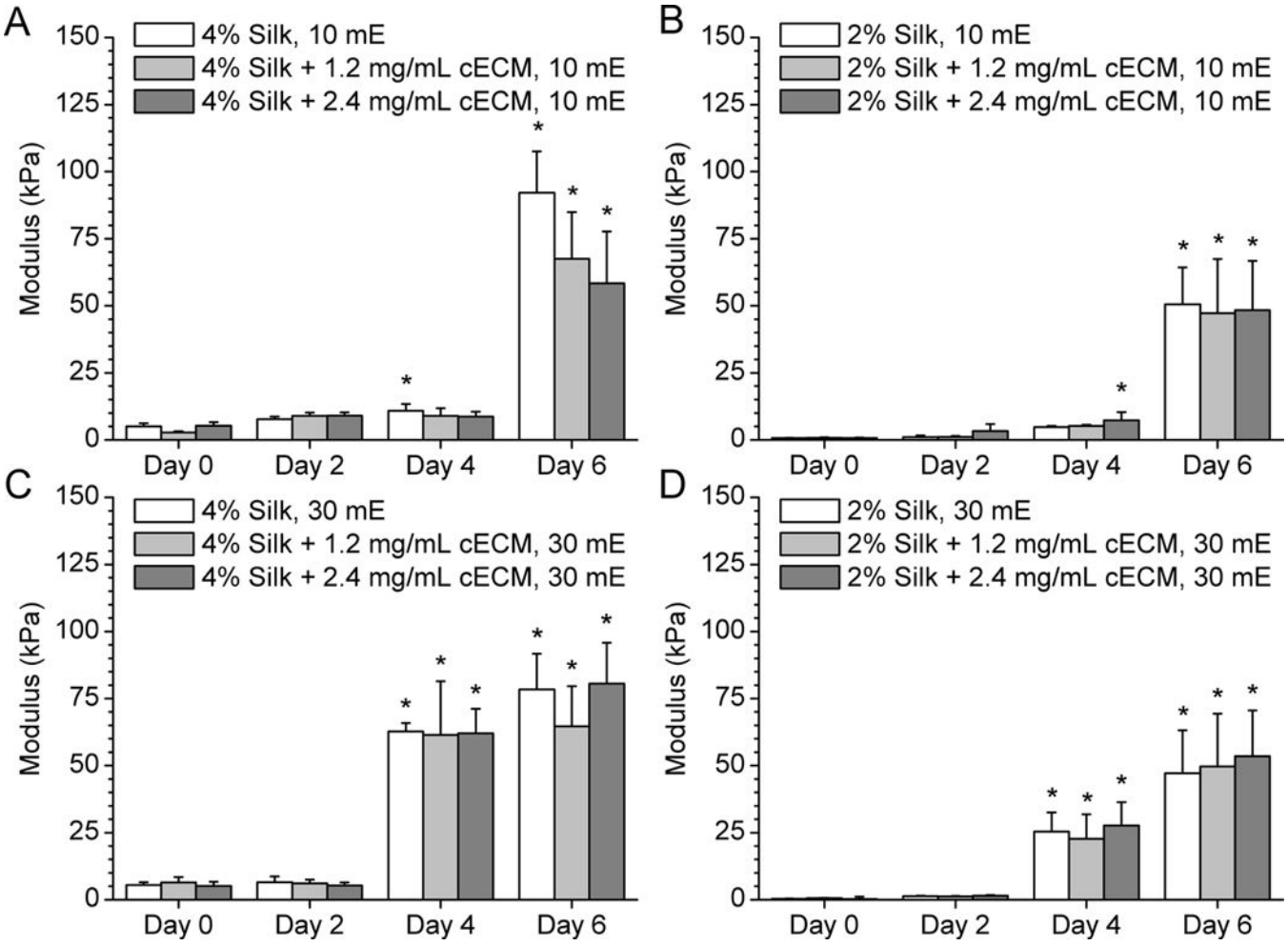

Figure 2. Modulus of silk hydrogels over time is not affected by the addition of the cECM

A) 10 minute extracted 4% silk hydrogels with either 0, 0.12% or 0.24% cECM show substantial stiffening between days 4 and 6. B) 2% silk hydrogels ± cECM show minimal stiffening prior to day 4 followed by statistically significant stiffening by day 6. C) 30 mE silk stiffens more quickly, showing a significant change in modulus between day 2 and day 4. The differences in the rates of stiffening are a result of the change in polymer chain length and the role chain length plays in silk fibroin crystallization. All values were calculated from the slope of unconfined compression at 10% strain per minute between strains of 20% and 30% and are reported ± standard deviation. Statistical differences between samples are denoted with an asterisk, which represents statistically greater average value compared to that condition's day 0 average ($p < 0.05$). No statistical differences were noted with the addition of cECM when compared for each condition at each time point ($p > 0.05$).

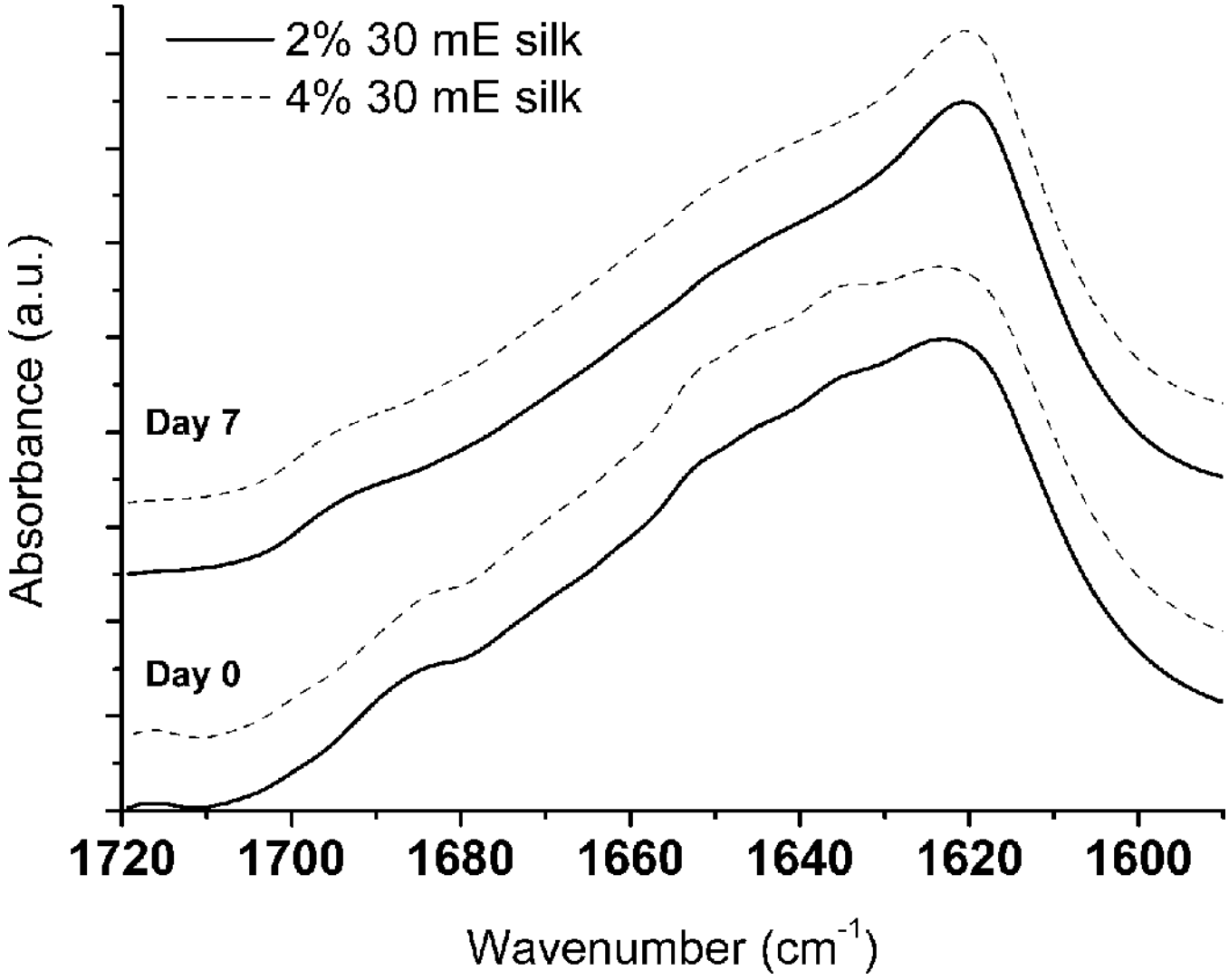

Figure 3. Representative FTIR spectra of 30 mE silk hydrogels

To evaluate the role of silk fibroin crystallization via changes in silk fibroin secondary structure within the samples, neat silk hydrogels were evaluated at day 0 and after 7 days in deuterated PBS. Qualitative evaluations of the spectra suggest that there is a change in silk fibroin conformation as evidenced by the change in peak shape between 1640 and 1620 cm^{-1}.

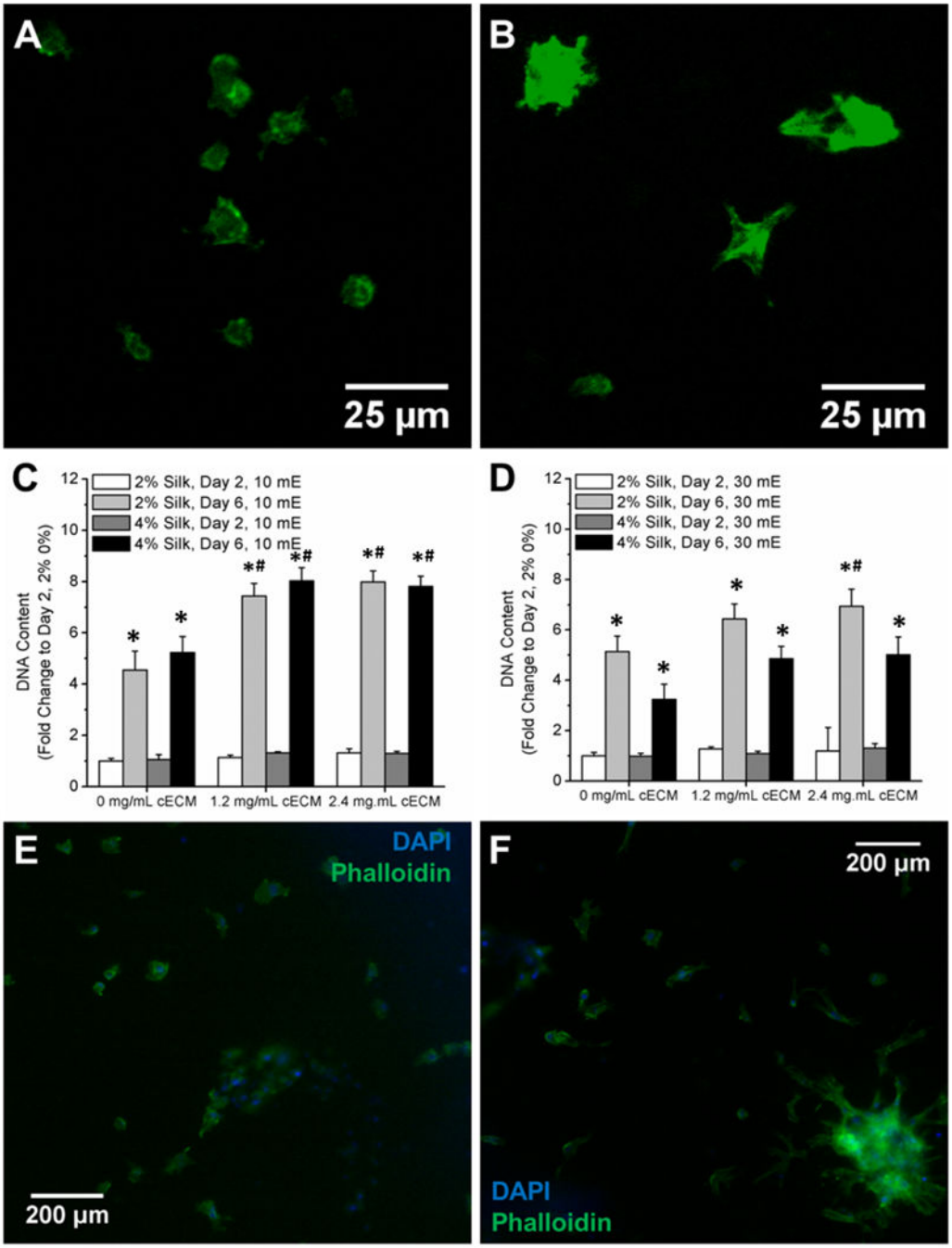

Figure 4. Evaluation of cell response to cECM addition within silk hydrogels

A) Live staining of cardiac fibroblasts within 2% 10 mE silk hydrogels after 2 days in culture. B) Live staining of cardiac fibroblasts within 2% 10 mE silk hydrogels with 2.4 mg/ml cECM after 2 days in culture. C) Fold change in DNA content within 10 mE silk hydrogels with and without cECM. DNA content significantly increases between day 2 and day 6 for all samples. Addition of cECM significantly increases the DNA content after 6 days within 10 mE silk samples. D) DNA content significantly increases after 6 days in culture for all samples. After 2 days in culture, cells within 10 mE silk samples were fixed

and stained with Phalloidin and DAPI to assess the actin network formation of the cardiac fibroblasts. Silk hydrogels without cECM (E) show less actin network formation compared to samples containing 2.4 mg/ml cECM (F). Asterisk (*) denotes samples that are statistically greater on day 6 compared to that same sample at day 2 ($p < 0.05$). Pound symbol ($^{\#}$) denotes samples that are statistically greater than the silk-only sample at that same time point ($p < 0.05$).

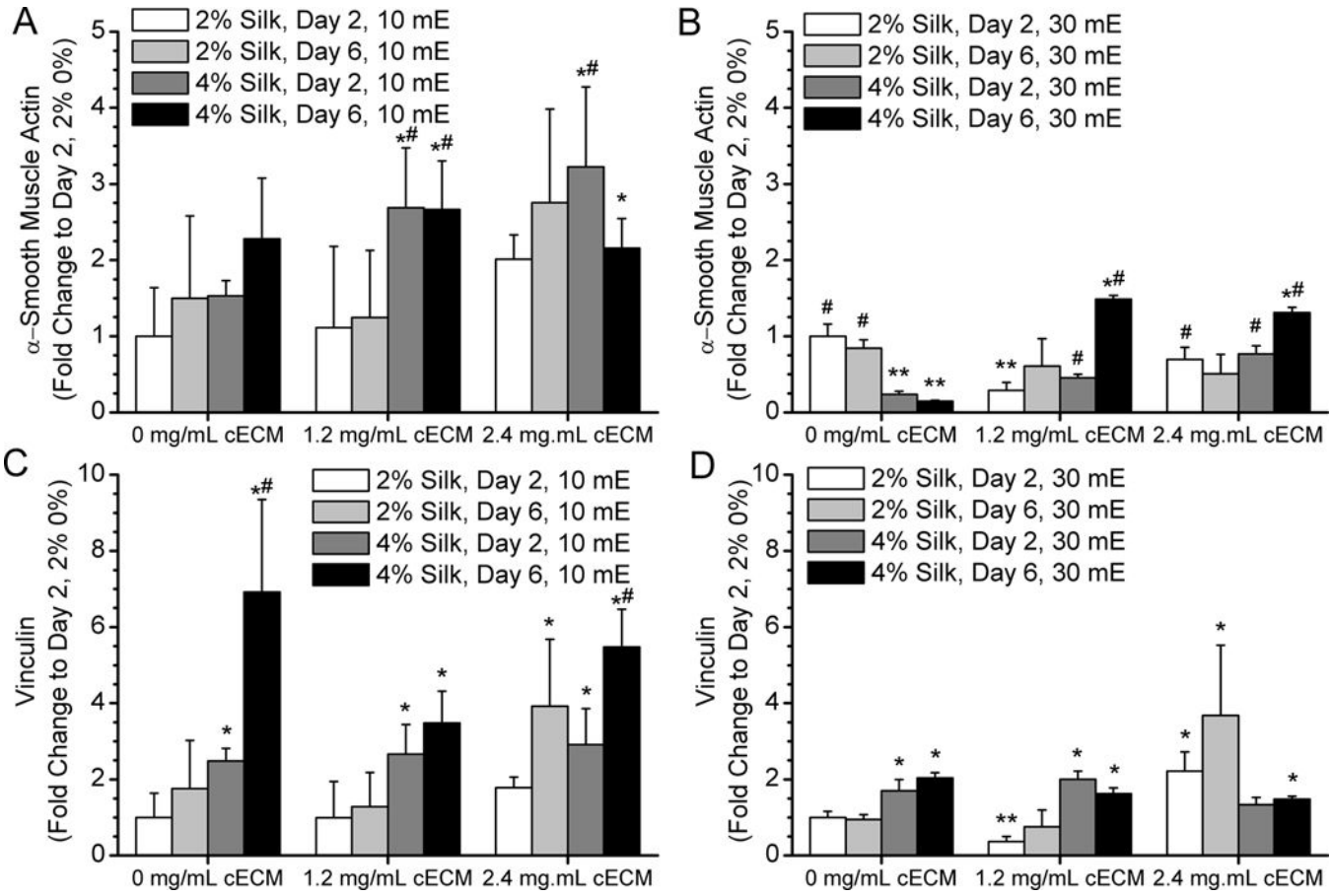

Figure 5. Protein expression by cardiac fibroblasts cultured within silk hydrogels

A) 10 mE silk with and without cECM show an increase in α-smooth muscle actin expression in samples containing cECM. B) 30 mE silk with and without cECM show an increase in a-smooth muscle actin expression in samples containing cECM. As a result of the stiffening of the hydrogel, cECM free samples decrease in expression over time. C) Vinculin expression by cardiac fibroblasts in 10 mE hydrogels increases over time and in samples with higher silk concentration. D) Vinculin expression is higher in 4% silk samples compared to 2% silk samples at day 2. However, the stiffening of the 30 mE silk samples does not lead to increased vinculin expression, suggesting that the stiffening of the samples limited CF growth and focal adhesion complex formation. Asterisk* indicates statistically greater protein expression compared to day 2 2% silk 0% cECM samples ($p < 0.05$). Pound symbol# indicates a significant increase in protein expression compared to day 2 4% silk 0% cECM samples ($p < 0.05$). Two asterisks** indicates a significant decrease in protein expression compared to day 2 2% silk 0% cECM samples ($p < 0.05$).

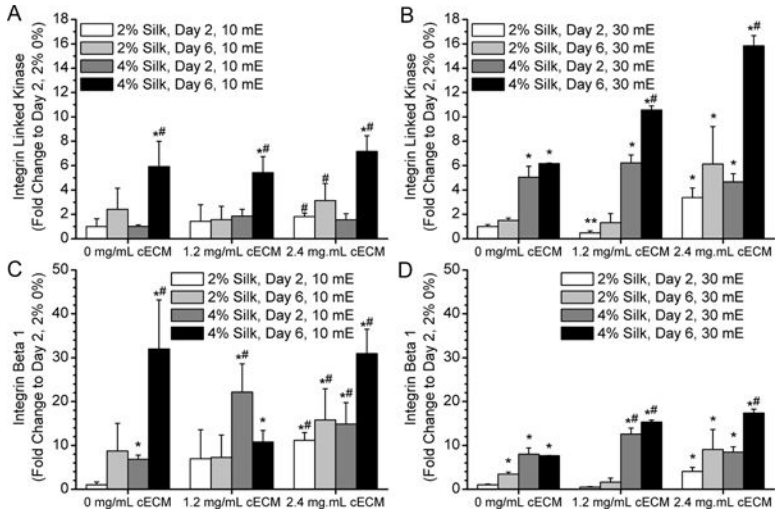

Figure 6. Integrin expression by cardiac fibroblasts cultured within silk hydrogels

A) 10 mE silk with and without cECM show an increase in integrin-linked kinase (ILK) expression over time. B) 30 mE silk with and without cECM show an increase in ILK expression as the samples stiffen, but the trend is more pronounced in samples containing cECM. C) Integrin β1 expression by cardiac fibroblasts in 10 mE hydrogels increases over time and in samples with cECM addition. D) Integrin B1 expression in 30 mE silk is higher in 4% silk samples containing cECM. Asterisk* indicates statistically greater protein expression compared to day 2 2% silk 0% cECM samples ($p < 0.05$). Pound symbol# indicates a significant increase in protein expression compared to day 2 4% silk 0% cECM samples ($p < 0.05$).

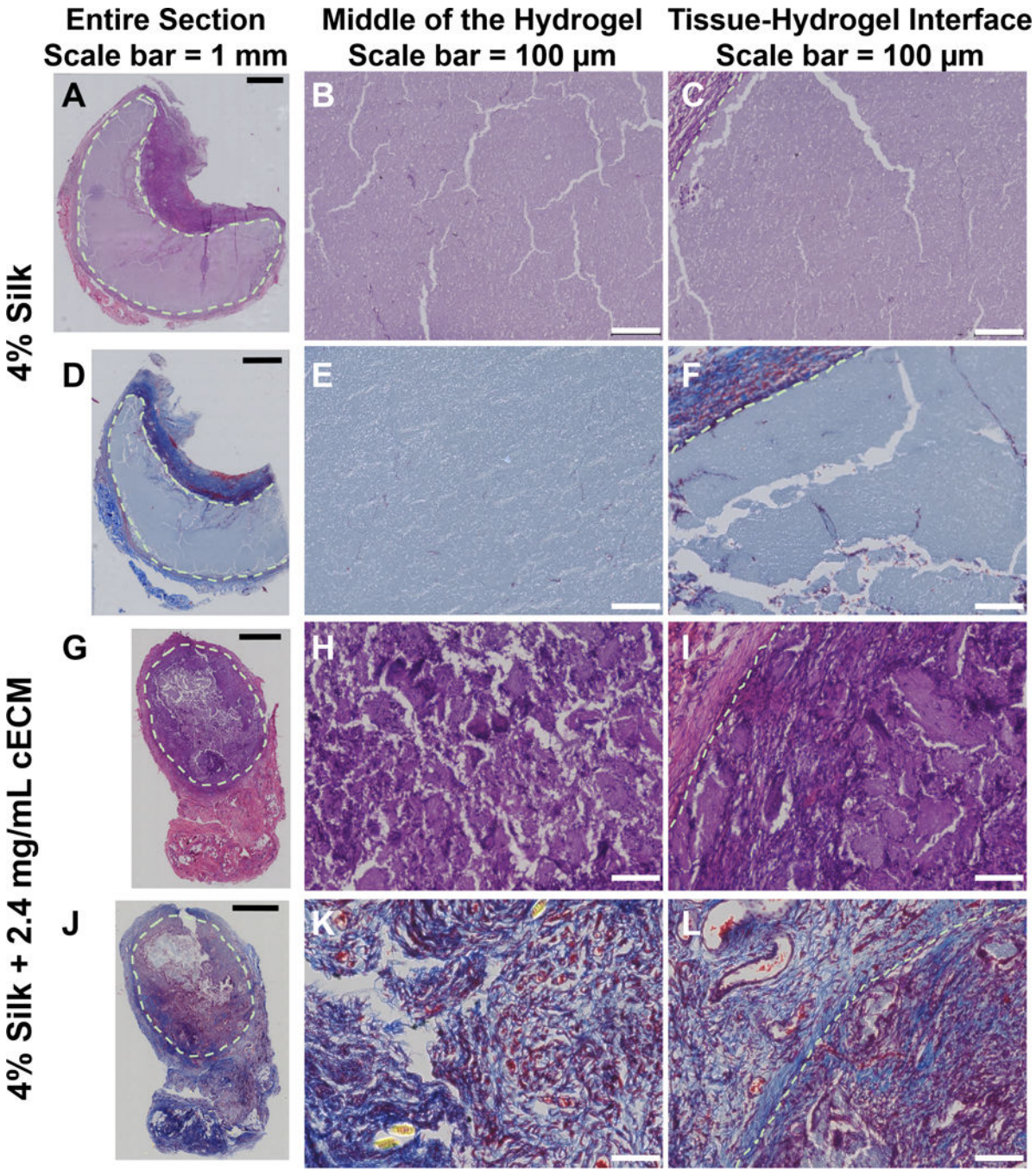

Figure 7. Qualitative evaluation of the role of cECM incorporation into silk hydrogels *in vivo*

Sections from 10 mE 4% silk only (A-F) and silk+ 2.4 mg/mL cECM (G-L) hydrogels were stained with Hematoxylin and Eosin (A-C, G-I) and Masson's Trichrome (D-F, J-L). The entire section is shown in the left hand column (A, D, G, J), a zoomed in image of the center of the scaffold is shown in the middle (B, E, H, K), and the tissue-hydrogel interface is shown on the left (C, F, I, L). Results indicated that cECM addition greatly improves cell infiltration.

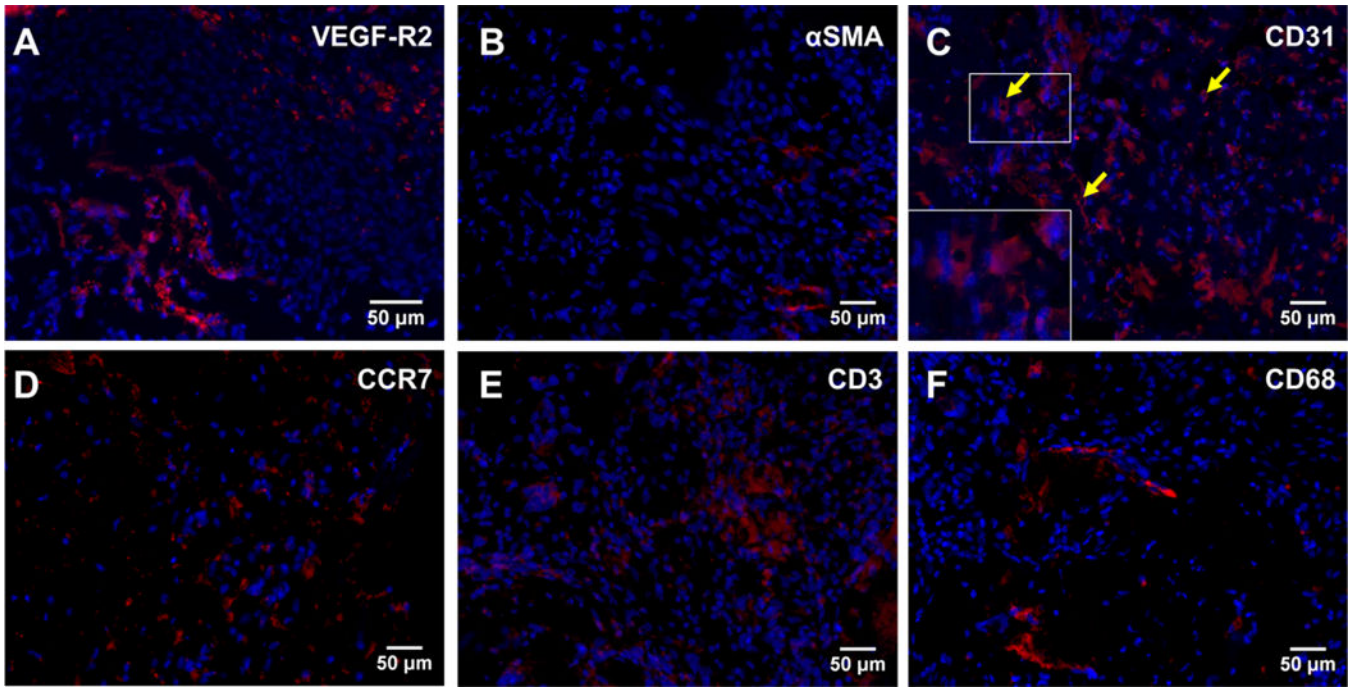

Figure 8. Evaluation of vascularization potential and macrophage infiltration following subcutaneous implantation

Middle sections from 10 mE silk+ 2.4 mg/mL cECM hydrogels were stained to determine the range of cell types that infiltrated into the sample. VEGFR-2 (A) stains cells participating in regeneration of vessel networks, such as blood or lymphatic vessels, alpha smooth muscle actin (αSMA, B) stains activated fibroblasts, and CD31 (PECAM-1, C) stains endothelial progenitors, endothelial cells, activated T-cells, and other cells types related vessel growth. The presence of the lumens in CD31 positive cells suggests that some of the infiltrating cells are of the endothelial lineage and have the potential to lead to vascularization following longer implantation studies. Yellow arrows in the CD31 image and inset denote to potential lumens. C-C chemokine receptor 7 (CCR7, D) is a marker of classically activated M1 phenotype, CD3 (E) labels activated T-cells, and CD68 is a pan-Macrophage marker (F). Evaluation of the middle of the injected hydrogels found areas positive for all of these markers.

Table 1

Formulations of silk hydrogels investigated in this study

To form the hydrogels, the first four components were added and mixed well. Hydrogen peroxide was added last, to initiate the crosslinking of hydrogels. For cell encapsulation experiments, the amount of media was adjusted to account for the volume needed to incorporate the cardiac fibroblasts. The fibroblasts were added 8 minutes following addition of H_2O_2, prior to gelation of the solution.

	Stock	Final concentration
Silk	4.5–6% wt/vol	2% or 4%
Supplemented DMEM	10 ×	0.5 ×
Horseradish peroxidase (HRP)	1000 units/ml_	15 units/mL
cECM	20 mg/mL	0, 1.2, or 2.4 mg/mL
Hydrogen Peroxide (H_2O_2)	1%	0.01%